PROCEEDINGS OF SPIE

SPIEDigitalLibrary.org/conference-proceedings-of-spie

# Higher density of ECM composition in pancreatic cancer correlates with reduced drug delivery

Cody Rounds, Sanzida Haque, Chengyue Li, Devin Nissen, Dhruv Ranjan, et al.

Cody C. Rounds, Sanzida Haque, Chengyue Li, Devin Nissen, Dhruv Ranjan, Marcella Vaicik, Rama S. Madhurapantula, Thomas C. Irving, Kenneth M. Tichauer, "Higher density of ECM composition in pancreatic cancer correlates with reduced drug delivery," Proc. SPIE 12357, Visualizing and Quantifying Drug Distribution in Tissue VII, 123570B (14 March 2023); doi: 10.1117/12.2650840

SPIE.

Event: SPIE BiOS, 2023, San Francisco, California, United States

Updated version 26 June 2023

# Higher density of ECM composition in pancreatic cancer correlates with reduced drug delivery

Cody C. Rounds *[a], Sanzida Haque [a], Chengyue Li [a], Devin Nissen [b], Dhruv Ranjan [a], Marcella Vaicik [a], Rama S. Madhurapantula [b,d], Thomas C. Irving [b,c,d], Kenneth M. Tichauer [a]
[a]Dept. of Biomedical Engineering, Illinois Institute of Technology, 3255 S Dearborn St Chicago IL 60616 [b]Dept. of Biology, Illinois Institute of Technology, 3101 S Dearborn St Chicago IL 60616 [c]BioCAT, Advanced Photon Source, Argonne National Laboratory, 9700 S Cass Ave Lemont IL 60439, [d]Pritzker Instt. of Biomedical Science and Engg., Illinois Institute of Technology, 3440 S Dearborn St Chicago IL 60616

## ABSTRACT

Pancreatic ductal adenocarcinomas (PDACs) are often treatment resistant, and as such widefield imaging methods for the evaluation of ECM composition are needed. Here we present a method to measure the relative abundance of ECM diffracting components in PDAC samples alongside drug penetration in widefield images. Orthotopic mouse PDAC xenografts are grown and assessment of drug penetration as well as ECM composition is done using co-registration of scanning x-ray diffraction (XRD) and EGFR-specific drug penetration fluorescent widefield images. Preliminary data suggests a strongly negative correlation between abundance of diffracting ECM components and penetration of large drugs in solid tumors. This methodology may be used to provide crucial insights into both drug-development approaches and multi-therapeutic treatment strategies in late stage PDAC patients presenting with ECM desmoplasia.

**Keywords:** Pancreatic ductal adenocarcinoma, scanning x-ray diffraction, widefield fluorescent imaging, tumor ECM analysis, molecular imaging

## 1. INTRODUCTION

Pancreatic ductal adenocarcinoma (PDAC) is almost uniformly lethal[1], with overall 5-year survival rates of ~8% that has remained constant over time[2] while global incidence is increasing.[3] For 80-90% of patients that present with PDAC in the clinic, the disease is already in late stages and a potentially curative surgical treatment is no longer an option, and instead are placed on neoadjuvant radiation and chemotherapy to limit the disease's growth and spread.[4] Over time, however, the disease will often grow resistant to these drugs and a more aggressive form will then dominate.[5] While there are many confounding factors that may contribute to this, the composition of the ECM is thought to be a major contributing aspect - it is generally accepted that the ECM composition plays the dominant role in restricting the delivery of these therapies.[6] As such, many new combination approaches to treatment propose the inclusion of ECM modeling drugs, in hopes that increasing/decreasing amount of specific ECM components may allow for better drug penetration and ultimately response. Despite those hypotheses, no technologies are currently capable of measuring ECM composition in large-field-of-view (millimeters) tumor sample imaging. A large-field-of view is important as it allows for visualization of intra-tumoral heterogeneities, which can lead to different portions of the tumor responding differently to the same drug. A view of the heterogeneities present in a tumor's ECM is critical to the development of curative mono or poly drug therapies, rather than temporary responses.

The phenomenon of dense, fibrotic ECM in PDAC patients is referred to as desmoplasia, and the primary components of the ECM that are modulated by the disease are collagens, specifically type I.[7] Collagen type I is a biopolymer that makes up >90% of the ECM in many tissues and is known to play a dominant role in pathophysiology of desmoplasia. This collagen type forms highly ordered fibrillar structures critical to maintenance of ECM mechanical integrity in healthy tissue. In PDAC, its overexpression brings about the formation of dense solid tumors where homogenous drug penetration is less likely.[8] Collagen I's fibrillar structure lends itself well to x-ray diffraction studies, as the known periodicity of its subunit repeats yields

Visualizing and Quantifying Drug Distribution in Tissue VII, edited by Kin Foong Chan, Conor L. Evans, Proc. of SPIE Vol. 12357, 123570B · © 2023 SPIE
1605-7422 · doi: 10.1117/12.2650840

characteristic diffraction patterns. By analyzing these diffraction patterns, it is possible to gain information about its relative abundance in a measured pathlength.[9]

Over expression of the Epidermal Growth Factor Receptor (EGFR) is another common feature in many PDAC cases and, given the FDA approval of the anti-EGFR monoclonal antibody cetuximab, this receptor is often a molecular target for many immunotherapy-based treatments in metastatic disease. Although cetuximab has seen high success in many cancer types, it has seen limited therapeutic effectiveness in treatment of metastatic PDAC.[10] This is thought to be largely due to the large molecular weight of the drug (150 kDa), which impairs its ability to penetrate the dense fibrillar tissue commonly seen in pancreatic neoplasms. This leads to a lower response to the drug as well as growth of PDAC lesions that express lower overall levels of EGFR, ultimately bringing about treatment resistance.

Newly approved near-infrared (NIR) dyes, which are preferable to visible dyes due to NIR's uniquely low interaction with tissue, have allowed for the synthesis of cetuximab-fluorescent dye conjugates for many molecularly guided imaging approaches. Conjugation of the antibody with a NIR fluorophore allows for visualization of the drug penetration into tissue, and as such, is an extremely useful tool for the generation of images with molecular-level contrast. This can be used toward investigating widefield drug specific binding, a measure that may be critical for the development of drugs, as well as managing treatment response in inoperable cases[11], in effect opening a window into drug resistance clinically[12].

## 2. METHODS

### *2.1 Tumor growth and fluorescent imaging*

$1x10^6$ human PANC-1 pancreatic adenocarcinoma cells were implanted into the pancreas of 10–14-week-old athymic mice. Orthotopic tumors were grown until they reached ~1 cm in diameter. 24 hours prior to euthanizing, 200 nanomoles of IRDye700-cetuximab conjugate was infused into the mice via tail-vein injection. The following day the portion of each pancreas with the tumor and its surrounding stroma was then resected out in-tact and underwent frozen sectioning at 500-micron thickness and mounted on Ultralene sheets for imaging. This mounted sample was then fixed on a slide mount for XRD scanning. A small black X was drawn onto the corner of each frozen section for later image registration purposes. The slices then underwent fluorescent NIR widefield imaging via the PEARL system (LI-COR Biosciences, Lincoln NE USA). The PEARL allows for co-registered white light images alongside images in the 700 channel, thus allowing for the location of the mark to be determined in the widefield fluorescent images. The samples were then stored on dry ice and transported to the synchrotron facility for scanning x-ray diffraction experiments.

### *2.2 Scanning X-ray Diffraction*

Scanning x-ray fiber diffraction was carried out at BioCAT, a high intensity x-ray beam line off the Advanced Photon Source located at Argonne National Laboratory. The experimental set up can be seen in **Fig 1**. Briefly, a beam was focused to an ~80-micron diameter point using mirrors. Sections of tumors embedded in OCT were mounted on a translating XY sample positioner, which positioned the portion of the sample from which XRD patterns were recorded on a Pilatus 1M detector (0.172 μm pixel size). The positioner was used to raster scan sections across each tumor with a step size of 0.1 mm between each datapoint. These diffraction patterns were then analyzed using the Diffraction Imaging program on the MuscleX software suite.[13] There the cumulative ring intensities were summed and placed into a matrix yielding a 2D widefield heatmap of the diffracting components in the sample. The diffraction heat maps were aligned with corresponding scanned area of the fluorescent images to allow for direct comparison between pixels of the same region in the sample. To reduce the contribution of noise, ROIs were drawn on the XRD heat map, followed by averaging of the

pixel values in each ROI for both the XRD map as well as the fluorescent image, and a cross comparison between the two was then done.

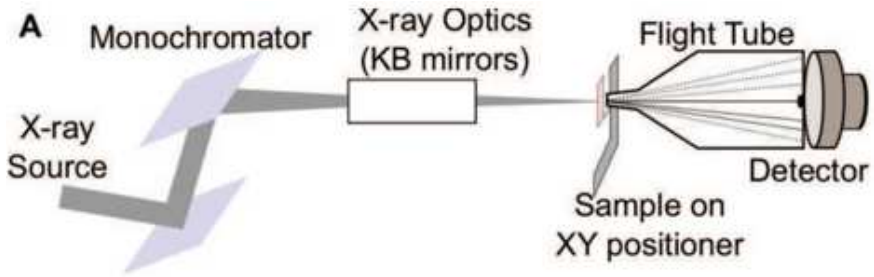


**Figure 1:** Schematic detailing the scanning XRD setup. X-rays pass from the beam line through a monochromator to yield a beam of narrow energy bandwidth. Photons then pass through a series of optics to focus the beam, which then pass through a mounted sample leading to beam diffraction. The diffracted rays then pass through a flight tube and the pattern is recorded onto a detector. Figure taken from Madhurapantula, et al.[9] with permission from authors.

## 3. RESULTS

Using a single specimen as an example, the white light image with corresponding black mark for registration and resulting XRD scanned area can be seen in **Fig.2A**. Corresponding 700 channel fluorescence of the scanned region is presented in **Fig.2B**, and the reconstructed XRD heat map can be seen in **Fig.2C** with the ROIs used for cross-correlation depicted as an overlay. Results of the cross correlations between XRD heat map and fluorescent images for 3 samples can be seen in **Fig.3A-C**. Line of best fit was plotted alongside the data points, indicating an overall negative correlation for all three samples.

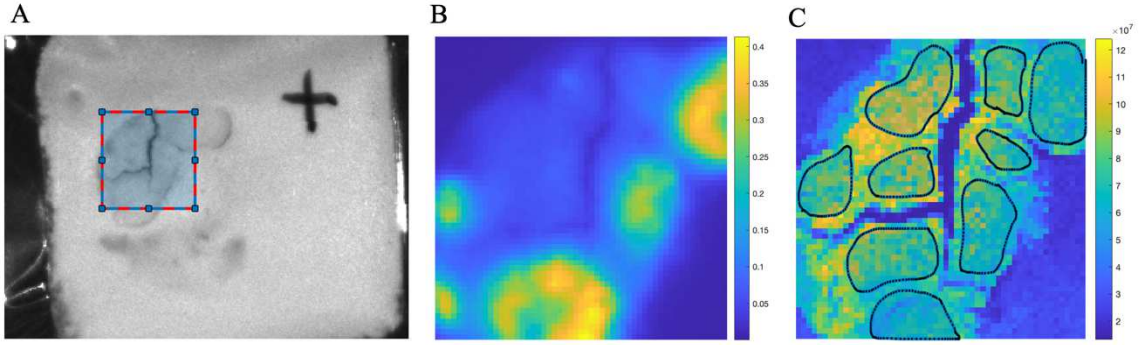


**Figure 2:** A) White light image of the whole specimen, embedded in OCT and cryo-sectioned at 500-micron thickness. Mark used for image registration in black, which alongside XRD scanning stage absolute position coordinates, was used to calculate the scanned area noted as a shaded box. B) The 700 nm channel, corresponding to the widefield fluorescence of the scanned region. C) XRD heatmap of the same noted scanned region, with all analyzed ROIs overlaid.

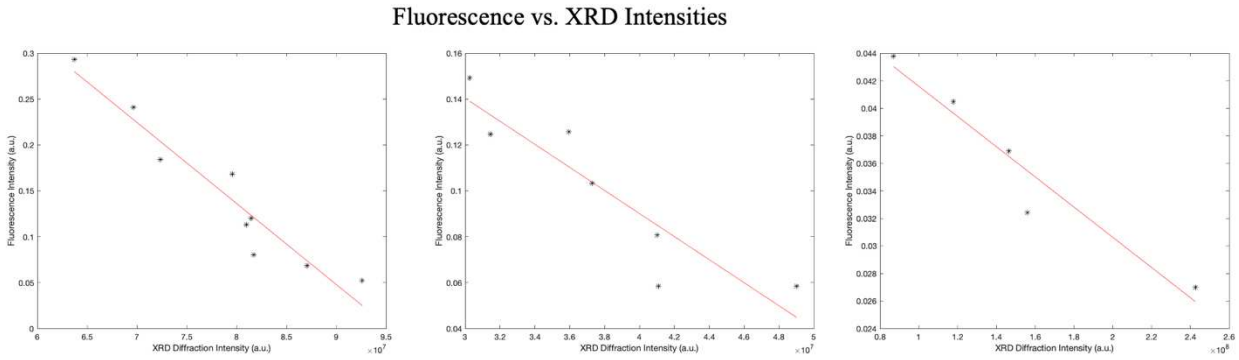


**Figure 3**: Cross correlation results for 3 different samples (A-C). Each data point, noted in black, indicates the mean pixel intensity of ROIs in both the fluorescence image (drug penetration, y-axis) versus XRD (diffracting ECM components, x-axis) heat map. An overall negative correlation is indicated across all 3 samples, with correlation coefficients ($R^2$) for A, B, and C equal to 0.92, 0.83, and 0.93, respectively.

## 4. DISCUSSION

These preliminary results demonstrate a negative correlation between large molecular weight drug penetration and abundance of ECM components capable of diffracting x-rays. While the XRD analysis conducted here was not collagen-specific, it is assumed that the primary diffracting component of the ECM is collagen type-I. This can be verified in a future analysis, where the XRD rings associated with collagen type-I d-spacing are the only rings selected and their intensities compiled into the heat map. In addition to assessing the abundance of purely collagen, it is also possible to assess the relative penetration of multiple different drugs using this methodology, granted one has access to a widefield fluorescent imaging system capable of imaging in multiple channels. The PEARL can accommodate fluorescence in both the 700 and 800 channels, permitting the potential use of this methodology to compare penetration of two different co-administered drugs alongside the associated density of tumor stroma via XRD. In these the use of paired-agent studies may further be used to quantify the binding potential of drugs to different tumor regions in the widefield. This can be used to open a window into drug specific binding[14], with alongside measurements of tumor stroma density can provide critical information about drug development, a metric important for increasing overall treatment response. Poly therapeutic treatment strategies may be further employed to investigate the effects of ECM modeling drugs on modulating the specific binding kinetics of chemotherapies.

## 5. ACKNOWLEDGEMENTS

This work was funded by NSF CAREER Award (1653627) and the Nayar Prize at Illinois Tech. Access to the synchrotron beamline was provided by Dr. Thomas Irving and data analyses assistance was provided by Dr. Joseph Orgel and team.

Undergraduate student researcher (DR) was supported by the National Science Foundation – Research Experience for Undergraduates under award DMR 2050916.

## 6. REFERENCES


[1] Siegel, R. L., Miller, K. D. and Jemal, A., "Cancer statistics, 2016: Cancer Statistics, 2016," CA: A Cancer Journal for Clinicians **66**(1), 7–30 (2016).

[2] Australian Pancreatic Cancer Genome Initiative, Biankin, A. V., Waddell, N., Kassahn, K. S., Gingras, M.-C., Muthuswamy, L. B., Johns, A. L., Miller, D. K., Wilson, P. J., Patch, A.-M., Wu, J., Chang, D. K., Cowley, M. J., Gardiner, B. B., Song, S., Harliwong, I., Idrisoglu, S., Nourse, C., Nourbakhsh, E., et al., "Pancreatic cancer genomes reveal aberrations in axon guidance pathway genes," Nature **491**(7424), 399–405 (2012).

[3] Cui, J., Jiang, W., Wang, S., Wang, L. and Xie, K., "Role of Wnt/β-catenin Signaling in Drug Resistance of Pancreatic Cancer," CPD **18**(17), 2464–2471 (2012).

[4] Singh, R. R. and O'Reilly, E. M., "New Treatment Strategies for Metastatic Pancreatic Ductal Adenocarcinoma," Drugs **80**(7), 647–669 (2020).

[5] Du, J., Gu, J. and Li, J., "Mechanisms of drug resistance of pancreatic ductal adenocarcinoma at different levels," Bioscience Reports **40**(7), BSR20200401 (2020).

[6] Perez, V. M., Kearney, J. F. and Yeh, J. J., "The PDAC Extracellular Matrix: A Review of the ECM Protein Composition, Tumor Cell Interaction, and Therapeutic Strategies," Front. Oncol. **11**, 751311 (2021).

[7] Weniger, M., Honselmann, K. C. and Liss, A. S., "The Extracellular Matrix and Pancreatic Cancer: A Complex Relationship," Cancers (Basel) **10**(9), 316 (2018).

[8] Masugi, Y., "The Desmoplastic Stroma of Pancreatic Cancer: Multilayered Levels of Heterogeneity, Clinical Significance, and Therapeutic Opportunities," Cancers **14**(13), 3293 (2022).

[9] Madhurapantula, R. S. and Orgel, J. P. R. O., "X-Ray Diffraction Detects D-Periodic Location of Native Collagen Crosslinks In Situ and Those Resulting from Non- Enzymatic Glycation," [Accelerator Physics - Radiation Safety and Applications], I. Ahmad and M. Malek, Eds., InTech (2018).

[10] Forster, T., Huettner, F. J., Springfeld, C., Loehr, M., Kalkum, E., Hackbusch, M., Hackert, T., Diener, M. K. and Probst, P., "Cetuximab in Pancreatic Cancer Therapy: A Systematic Review and Meta-Analysis," Oncology **98**(1), 53–60 (2020).

[11] Meng, B., Folaron, M. R., Strawbridge, R. R., Sadeghipour, N., Samkoe, K. S., Tichauer, K. and Davis, S. C., "Noninvasive quantification of target availability during therapy using paired-agent fluorescence tomography," Theranostics **10**(24), 11230–11243 (2020).

[12] Ansari, D., Gustafsson, A. and Andersson, R., "Update on the management of pancreatic cancer: Surgery is not enough," WJG **21**(11), 3157–3165 (2015).

[13] Miskin, N. P., Ran, Xintian, Nabon, J., Nikseresht, G., Jiranun Jiratrakanvong, Iitbiocat, Prajwal Das, Prajwal Das, Xintian Lee and Tomirving., "biocatiit/musclex: v1.21.0" (2022).

[14] Tichauer, K. M., Samkoe, K. S., Sexton, K. J., Hextrum, S. K., Yang, H. H., Klubben, W. S., Gunn, J. R., Hasan, T. and Pogue, B. W., "In Vivo Quantification of Tumor Receptor Binding Potential with Dual-Reporter Molecular Imaging," Mol Imaging Biol **14**(5), 584–592 (2012).